Journal of Fluids and Structures (1999) **13,** 429–442
Article No.: jfls. 1999.0216. available online at http:/www.idealibrary.com on IDEAL

FLOW STRUCTURE AND VARIATION OF WALL SHEAR STRESS IN ASYMMETRICAL ARTERIAL BRANCH

R. YAMAGUCHI

Department of Mechanical Engineering, Faculty of Engineering, Shibaura Institute of Technology, Tokyo, 108 Japan

(Received 13 May 1997 and in revised form 3 October 1998)

In the present study, the flow structure such as the velocity profile and the wall shear stress in an asymmetrical arterial branch in laminar steady flow has been experimentally studied. In the branch model, the daughter tube asymmetrically bifurcates from the parent tube at 45°. The axial and the transverse velocity components have been measured by two-dimensional laser Doppler velocimetry, and the wall shear stress is measured by the electrochemical method. Furthermore, the wall shear stress estimated from the velocity profile is compared with that measured by the electrochemical method. Consequently, it has been clarified that, as it approaches the entrance of the daughter tube, the core flow deflects into the daughter tube, and the variation of wall shear stress along the proximal wall results from the secondary motion which is transferred from the parent tube to the daughter tube.

1. INTRODUCTION

HEMODYNAMIC FACTORS such as wall shear stress, vortex generation, turbulence, and oscillation shear index have been considered to be important for the initiation and the development of the arterial disease according to Stehbens (1959), McDonald (1974), and Ku *et al.* (1985). The atherosclerotic lesion initiates in strongly disturbed regions, such as in the aortic arch and the arterial branch. The asymmetrical arterial branch in which the renal and the mesenteric arteries bifurcate from the abdominal aorta is one of the predilection sites of the disease. Particularly, the development of atherosclerosis may be closely related to the physiological response of arterial wall to wall shear stress. Therefore, the wall shear stress is the most important hemodynamic factor affecting the interface between blood flow and arterial wall.

Concerning atherosclerotic disease at the arterial branch, several views have been obtained from experiments on animals and the pathological observations of Cornhill *et al.* (1985), Kjaernes *et al.* (1981) and Friedman *et al.* (1981). Disease occurs along the proximal wall of the daughter tube in large animals. The site of disease varies in each experiment, and this variation of disease site may be related to the flow pattern and the flow division ratio into each downstream tube. Yoshida *et al.* (1987) and Yamaguchi *et al.* (1986) have indicated in their recent studies that atherosclerotic disease in the inferior mesenteric artery proliferates at the proximal wall, where the wall shear stress would be lower than that around the flow divider.

The mesenteric artery which bifurcates from the abdominal aorta is one of the typical asymmetrical branches. Lutz *et al.* (1977) and El Masry & Feuerstein (1982) measured wall shear stress in the three-dimensional mesenteric branch with a daughter tube bifurcating

0889–9746/99/040429 + 14 $30.00

from a parent tube asymmetrically. They suggested that the wall shear stress along the proximal wall of the daughter tube is not necessarily low, it varies in magnitude, and the variation of wall shear stress might be associated with the site of arterial disease. Rodkiewicz & Roussel (1973) have indicated that in the asymmetrical branch there exist two interdependent flow separation regions in each downstream tube and some of the fluid from the separation region in the parent tube is transferred into the daughter tube.

In a previous study, Yamaguchi & Kohtoh (1994) studied the flow structure through an asymmetrical branch in which the daughter tube bifurcates from the parent tube at 45° with a large radius of curvature at the round upstream corner of the daughter tube, i.e., the radius of curvature is 3·5 times as large as the diameter of the parent tube. Using the electrochemical method suggested by Mizushina (1971) and applied by Yamaguchi (1989), they clarified that the wall shear stress along the proximal wall, around the round upstream corner, varies in the form of a damped sinusoidal wave, i.e., the wall shear stress exhibits at least two maxima and two minima and its amplitude damps downstream. Also, using flow visualization, they have qualitatively supported that this sinusoidal variation is induced by a secondary helical flow from the parent tube to the daughter tube. This variation of wall shear stress is the first observation clarified by the authors in the previous study. Therefore, it would be desirable to verify the variation along the proximal wall and the wall shear stress measured by the electrochemical method with another method. Furthermore, it is necessary to evaluate the secondary flow quantitatively, which affects the variation of wall shear stress. In general, the flow structure strongly depends on geometrical factors, such as the radius of curvature at the upstream corner and the branch angle.

In the present study, an asymmetrical branch in which the daughter tube bifurcates from the parent tube at 45° with the same radius of curvature as the diameter of parent tube is investigated. The axial and the transverse velocity components are measured by laser Doppler velocimetry, and the wall shear stress is directly measured by the electrochemical method. Consequently, it is clarified that the wall shear stress steeply varies around the upstream corner and this variation is induced by the secondary transverse flow from the parent tube to the daughter tube. Furthermore, the wall shear stress estimated from the axial velocity component near the tube wall at the common median plane is compared with that measured by the electrochemical method.

2. EXPERIMENT

2.1. Branch Model and Measurement Section

The branch model employed in the present study is shown in Figure 1(a). The working fluid flows into the branch model through a straight tube with inlet length of 2·5 m from a constant head tank. The daughter tube of $D_1 = 14$ mm diameter asymmetrically bifurcates at 45° from the parent tube of $D_0 = 24$ mm diameter with the radius of curvature $R_D = D_0$ at the upstream corner. Although the branch geometry is similar to that in the previous study, the radius of curvature $R_D = D_0$ is different from $R_D = 3{\cdot}5D_0$ in the previous one, and this difference should greatly affect the flow structure.

The junction surface between the parent and the daughter tubes is smoothly connected as shown in Figure 1(b). A_i, B_i, E_i, and F_i denote the measurement positions of wall shear stress. A_i is along the outer wall of the parent tube, B_i is along the proximal wall, E_i is along the distal wall of the daughter tube, and F_i is along the inner wall of the parent tube. In total, the wall shear stress at the common median wall is measured by the electrochemical method at 132 points. Q_T and Q_D denote the flow rate through the upstream parent and the daughter tubes, respectively.

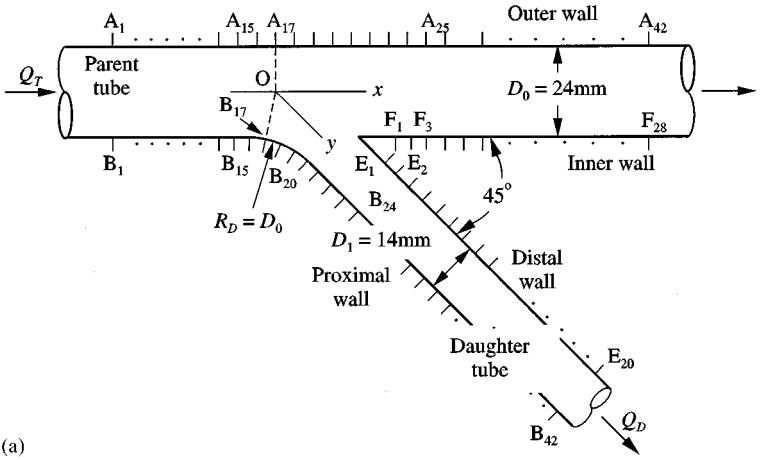

(a)

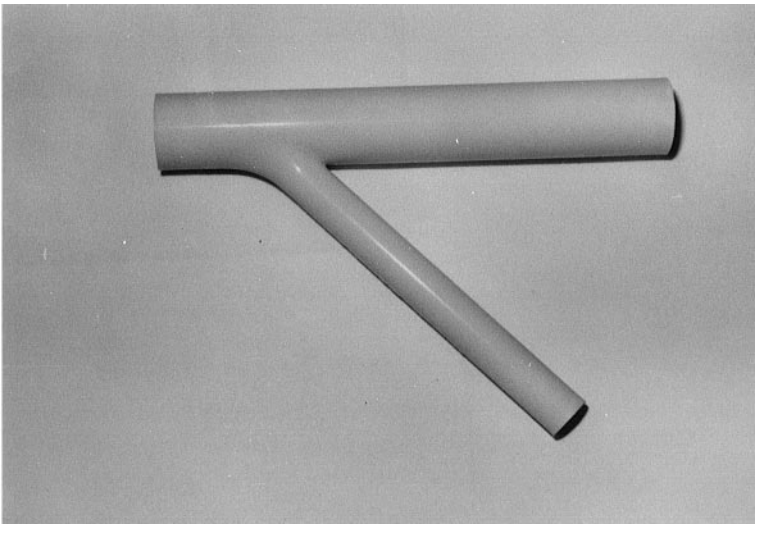

(b)

Figure 1. (a) Sketch of flow field and electrodes arrangement in 45° asymmetrical branch model with radius of curvature ($R_D = D_0$); (b) cast of 45° asymmetrical branch model.

2.2. Measurement of Velocity Profile and Flow Visualization

The coordinate system and the section of velocity measurement are shown in Figure 2. The plane which includes both axes x and ξ is defined as the common median plane and is set up horizontally in the experiment. The coordinates y and η are perpendicular to the parent tube axis x and the daughter tube axis ξ at the common median plane, respectively. Axis z is normal to the common median plane in both tubes. The velocities v_x and v_ξ denote the axial velocity component in the parent and the daughter tubes, respectively. On the other hand, the velocities v_y and v_η denote the secondary transverse velocity component in y and η, respectively.

The velocity profile is mainly measured for the model $R_D = D_0$ at several sections where the wall shear stress varies markedly, i.e., P_{-2} (A_2-B_2, $x/R_0 = -8{\cdot}6$) in the upstream parent tube, P_{-1} (A_{15}-B_{15}, $x/R_0 = -0{\cdot}9$) at the transition section from the straight upstream parent tube to the round upstream corner, $P_{1,2,3}$ in the downstream parent tube, $M_{1,2,3}$ in the daughter tube, and $B_{16,17,18,19,20}$ along the round proximal wall.

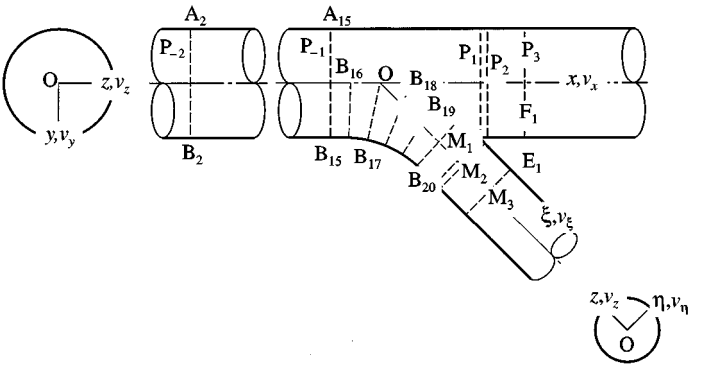

Figure 2. Coordinates, velocity components and measurement section of velocity profile ($R_D = D_0$).

The working fluid employed in the experiment is saturated aqueous potassium thiocyanate (KSCN) solution. The refractive index of this working fluid is almost the same as that of the Plexiglas, and therefore the difference of the refractive index between the channel material, Plexiglas, and the working fluid can be neglected. At a temperature of 295 K, the properties of the working fluid are: refractive index, $n = 1{\cdot}49$, density, $\rho = 1{\cdot}44$ g/cm^3, and kinematic viscosity, $v = 2{\cdot}18 \times 10^{-6}$ m^2/s.

The velocity profile is measured by two-dimensional laser Doppler velocimetry in the backscatter mode. The focal length of the convex lens is 122 mm, and the shape of the sampling volume of each beam is regarded as a prolate spheroid with diameter of about 40 μm and length of about 200 μm in the atmosphere according to the TSI specifications. Owing to the difference of refractive index between the working fluid and the atmosphere, the length of the sample measuring volume is about 300 μm in the working fluid. The diameter of measuring volume in the working fluid is approximately equal to that in the atmosphere, i.e., 40 μm.

The measurement of the axial and the transverse velocity components is carried out across the tube diameter both at the common median plane and normal to it. The velocity profile is measured every 1 mm across both diameters. Since the laser beams enter perpendicular to the common median plane, the space resolution of the present laser Doppler velocimetry system is 40 μm for the measurement at that plane. The velocity near the tube wall, i.e., within a distance of 1 mm from the tube wall, is measured every 0·2 mm.

The traverse position is controlled every 5 μm by the stepping motor. Consequently, the precision of the positioning system is 5 μm. In the measurement, the measuring volume position with respect to the tube wall could be determined with an accuracy of 0·02 mm by observing the Doppler signal on the oscilloscope. Therefore, the precision of the measuring volume position with respect to the tube wall would be 0·02 mm. The wall shear stress is calculated by assuming a linear variation in velocity between the tube wall and a position h = 0·4 mm from the wall. So, the measurement error of wall shear stress caused by the deviation of measuring volume position is estimated to be $\varepsilon_1 = 5\%$. It is possible to estimate the effect of the linear fit on the true value τ_i in regions of the Poiseuille flow. The wall shear stress τ_i in Poiseuille flow upstream in the parent tube is exactly obtained as follows:

$$\tau_i = 8\rho v U / D_0,$$

where U is the mean cross-sectional velocity in the upstream parent tube and v is the kinematic viscosity of the working fluid. On the other hand, the wall shear stress τ_l calculated in linear fit from the velocity at the distance of h from the tube wall is theoretically

obtained as follows:

$$\tau_l = 8\rho\nu U/D_0(1 - h/D_0);$$

so, the error ε_2 based on the linear fit for Poiseuille flow is

$$\varepsilon_2 = \frac{\tau_l - \tau_i}{\tau_i} = -\frac{h}{D_0} = -\frac{0{\cdot}4}{24}$$

$$= -0{\cdot}017\ (2\%).$$

The wall shear stress calculated from the linear fit is underestimated by 2%. In general, the error in wall shear stress measurement by the laser Doppler velocimetry is assumed to be $\varepsilon_1 + \varepsilon_2 = 7\%$.

The streamline at the common median plane is visualized by the polystyrene particles projected laser sheet. Also, the general flow pattern is visualized by the dye injected from the parent tube upstream of the branch point, composed of 90% black ink and 10% methylene blue.

2.3. Measurement of Wall Shear Stress by the Electrochemical Method

In the measurement of wall shear stress, an electrolytic solution composed of 0·01 M potassium ferricyanide $K_3Fe(CN)_6$, 0·01 M potassium ferrocyanide $K_4Fe(CN)_6$ and 1·0 M potassium hydroxide KOH as a supporting electrolyte is employed as the working fluid. The properties of this working fluid are approximately the same as those of the distilled water, i.e., density, $\rho = 1{\cdot}044\ \mathrm{g/cm^3}$, and kinematic viscosity: $\nu = 0{\cdot}839 \times 10^{-6}\ \mathrm{m^2/s}$ at a temperature of 303 K. The wall shear stress has been directly measured using the electrochemical method which is based on a diffusion-controlled reaction of ferricyanide ion to ferrocyanide ion at a platinum electrode with diameter 0·5 mm. Wall shear stress is proportional to the cube of electric current flowing between each test electrode and the counter electrode (Mizushina 1971; Yamaguchi 1989).

3. RESULTS AND DISCUSSION

Experiments have been carried out in steady flow, i.e., the Reynolds number of $\mathrm{Re} = UD_0/\nu = 800$ and the geometrical flow division ratio $Q_D/Q_T = 0{\cdot}25$, proportional to the cross-sectional ratio $D_1^2/(D_0^2 + D_1^2) = 0{\cdot}25$. The flow condition at $\mathrm{Re} = 800$ simulates the maximum flow rate at the systolic phase in the abdominal aorta. The "resting" or "post-prandial" state may relate to the flow division ratio. The geometrical flow division ratio $Q_D/Q_T = 0{\cdot}25$ will correspond to the resting state.

3.1. Flow Visualization

The flow pattern visualized by dye and particle tracking is shown in Figure 3(a–c). OW, IW, PW, and DW denote the outer, inner, proximal and distal walls, respectively. The dye injected from the outer wall of the upstream parent tube separates near the branch point as shown in Figure 3(a). As displayed in this figure, one of the dye streaks progresses downstream in the parent tube. The other dye streaks flow upstream along both side walls of the parent tube, and then after impinging on the round proximal wall, they flow into the daughter tube as a pair of helical streaks, as described by Rodkiewicz and Roussel (1973). The dye injected from the core flow above the common median plane flows into the daughter tube with some skewing as shown in Figure 3(b), and then flows downstream in

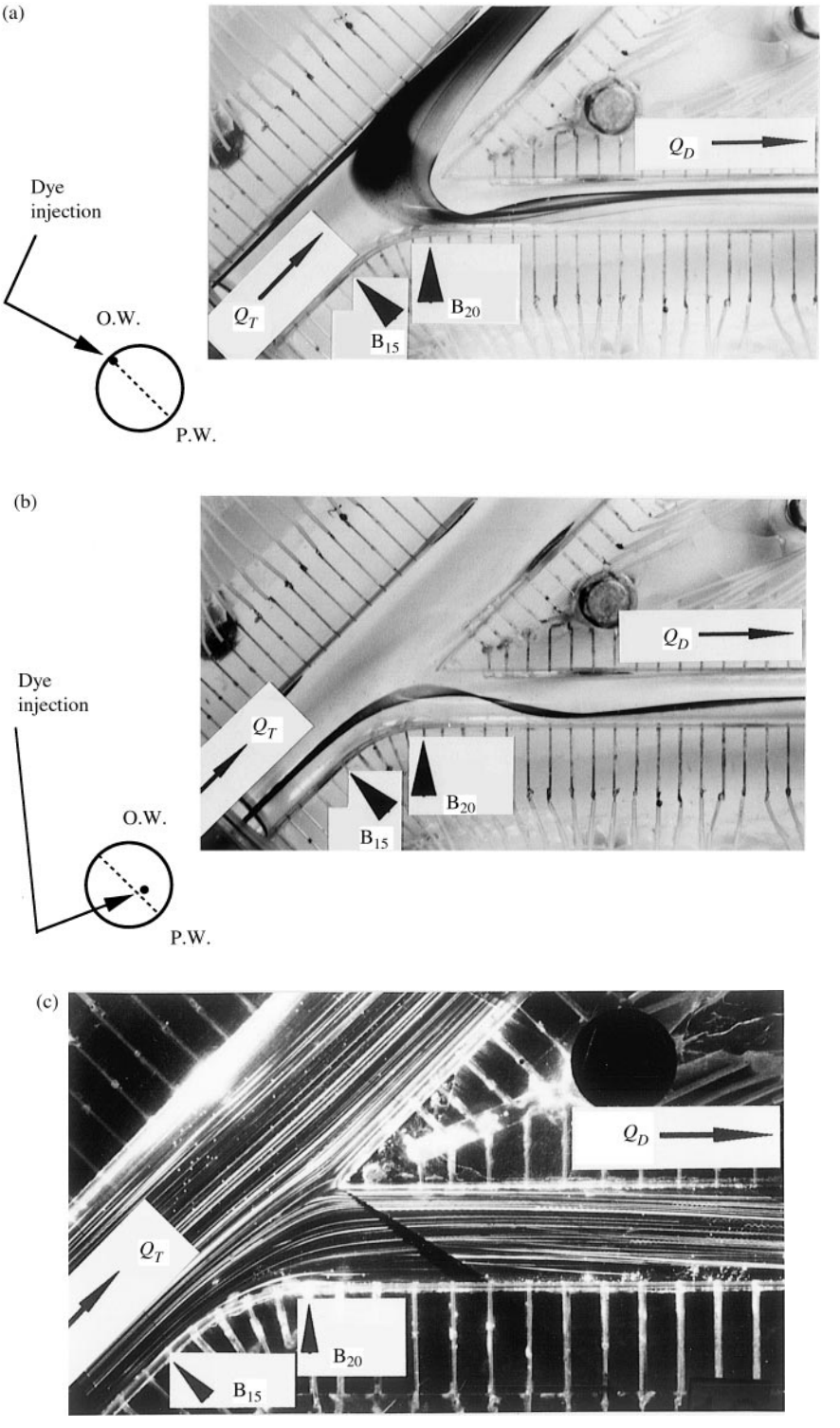

Figure 3. Flow visualization results: (a) dye streamline from outer wall of parent tube; (b) dye streamline from core flow above common median plane; (c) particle streamline at common median plane. Dotted line: common median plane, Re = 820, $Q_D/Q_T = 0{\cdot}30$.

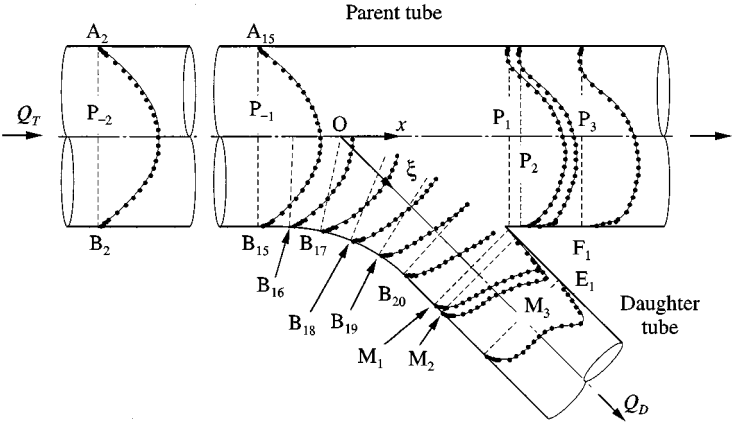

Figure 4. Axial velocity profile at common median plane (Re = 800, $Q_D/Q_T = 0{\cdot}24$).

a helical pattern. The streamline at the common median plane is shown in Figure 3(c). There is no flow separation along the proximal wall in the daughter tube.

3.2. Axial Velocity Profile

The axial velocity profile in the whole field at the common median plane is shown in Figure 4. At the upstream section P_{-2} ($x/R_0 = -8{\cdot}6$), the velocity profile is approximately parabolic. At the transition section P_{-1} ($x/R_0 = -0{\cdot}9$) from the straight upstream parent tube to the round upstream corner, the core flow begins to deflect into the daughter tube. The velocity gradient at the proximal wall ($y/R_0 = 1$) of the parent tube is much larger than that at the outer wall ($y/R_0 = -1$). In section P_2 ($x/R_0 = 2{\cdot}0$) 2·0 mm downstream of the flow divider, the velocity gradient along the inner wall is remarkably high and the velocity reaches the mean velocity of the upstream parent tube near the inner wall, $v_x/U = 1$. By contrast, separated reverse flow appears along the outer wall. Along the proximal wall around the upstream corner, the velocity gradually increases and the velocity gradient reaches a maximum value at B_{16}. Further downstream the velocity near the proximal wall decreases. In the present branch model, there is no flow separation along the proximal wall in the daughter tube. Along the distal wall, the velocity gradient at section M_1 near the flow divider reaches a maximum and then decreases downstream.

Therefore, there is no flow separation in the daughter tube at the geometrical flow division ratio. On the other hand, flow separation exists along the outer wall of the parent tube.

The axial velocity profile at the z-axis normal to the common median plane is shown in Figure 5. Poiseuille flow is found in the upstream parent tube. Although the velocity in the downstream parent tube is maximum at the tube axis, the velocity profile is not exactly symmetric. This asymmetry might be due to thermal convection owing to the temperature difference between the room temperature and the temperature of the working fluid. The velocity in the daughter tube displays the typical M-shaped profile.

The velocity obtained by laser Doppler velocimetry exhibits a random fluctuation in laminar steady flow. The time-averaged axial velocity at the upstream parent tube axis is 0·142 m/s at the Reynolds number of 800. From the random fluctuation at the tube axis, the standard deviation is estimated to be 0·011 m/s. Therefore, the coefficient of variation which is the ratio of the standard deviation to the time-averaged axial velocity is 7·5%.

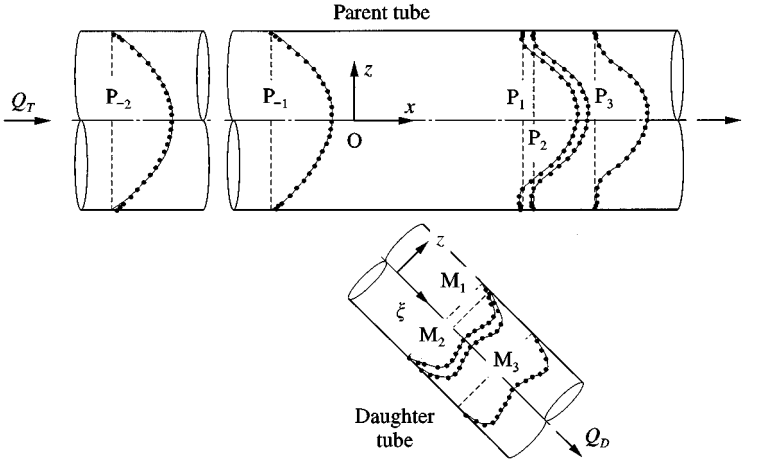

Figure 5. Axial velocity profile at the z-axis normal to common median plane (Re = 800, $Q_D/Q_T = 0{\cdot}24$).

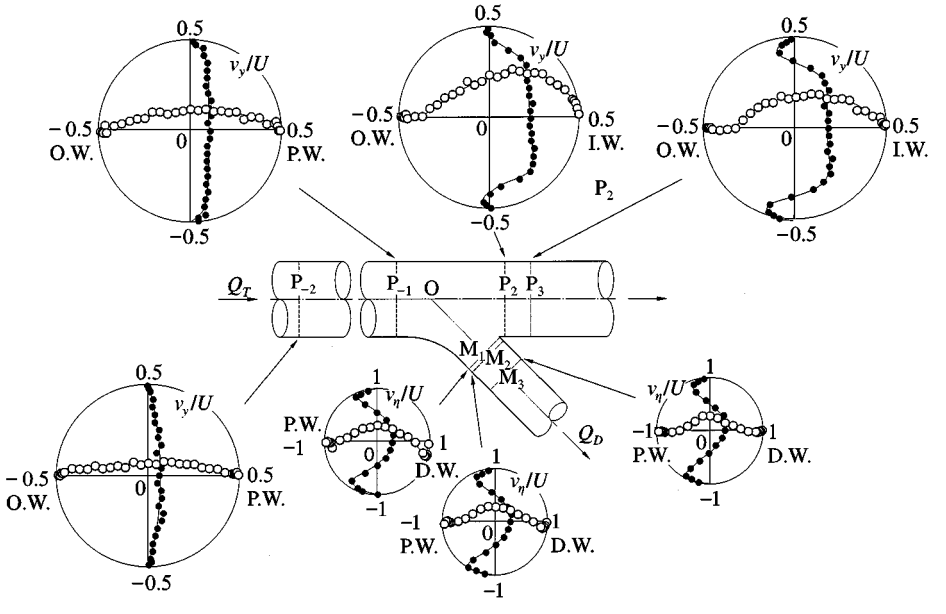

Figure 6. Transverse velocity profiles (Re = 800, $Q_D/Q_T = 0{\cdot}24$) Symbols ○ and ● denote the velocity at common median plane and at the z-axis normal to common median plane, respectively.

3.3. Transverse Velocity Profile

The whole transverse velocity profile is shown in Figure 6. The open and closed (dark) circles denote the transverse velocity at the common median plane and at the z-axis normal to the common median plane, respectively. The velocities v_y and v_η are the transverse velocity components in the parent and the daughter tubes, respectively. Although at section P_{-1} the flow direction of the closed symbol (●) coincides with that in figure, the flow direction of the open symbol (○) differs from the actual direction. After rotating 90° clockwise, the flow direction of the open symbol coincides with the actual flow direction. So, the transverse flow direction at section P_{-1} is from left to right across the whole cross-section, i.e., from the outer wall to the proximal wall.

Secondary flow from the outer wall to the proximal wall is already present at the upstream section P_{-2} ($x/R_0 = -8{\cdot}6$). At the transition section P_{-1}, the magnitude of the transverse velocity at the tube axis is 10% of the mean axial velocity in the upstream parent tube. In the daughter tube, a symmetrical pair of secondary vortices is evident. At section M_1, the magnitude of the transverse velocity at the tube axis reaches $0{\cdot}3U$. At this section another small secondary vortex appears along the distal wall. At the common median plane in the downstream parent tube, the flow near the outer wall is directed from the core region toward the outer wall. On the contrary, the core flow deflects toward the inner wall. At the z-axis normal to the common median plane, the core flow is directed into the inner wall, and the fluid along both side walls, apart from the core flow, is directed into the outer wall. Therefore, two pairs of secondary vortices exist in both downstream tubes. At section P_2, the magnitude of the transverse velocity at the tube axis reaches $0{\cdot}2U$.

3.4. Distribution of Wall Shear Stress

The wall shear stress estimated from the velocity profile near the tube wall is compared with that measured by the electrochemical method in Figure 7(a) for the case of $R_D = D_0$. The open symbols, i.e., wall shear stress measured by the electrochemical method is given in only the absolute value, since this method is not able to detect the flow direction. The closed symbols denote wall shear stress estimated from the velocity at the common median plane. Left and right side figures indicate the distribution in the parent and in the daughter tubes, respectively. The wall shear stress τ_w is normalized by that of the Poiseuille flow upstream of the parent tube, i.e., $\tau_w = 1{\cdot}0$ denotes the wall shear stress of the Poiseuille flow upstream of the parent tube. τ_T, τ_P, and τ_D denote the asymptotic values in the upstream parent, the downstream parent, and the daughter tubes, respectively.

Along the outer wall of the daughter tube (A_i, △), the wall shear stress gradually decreases approaching the branch point. Downstream of the branch point, the distribution has inflection points near $x/R_0 = 1$ and 4. As indicated by the closed symbol (▲) and by flow visualization as shown in Figure 3(a), the wall shear stress is negative in the range $1 < x/R_0 < 4$ since the flow separates along the outer wall.

Along the proximal wall (B_i, ○), the wall shear stress steeply increases and reaches a maximum value $\tau_w = 2{\cdot}5$ near the transition point B_{16} from the straight parent tube to the round upstream corner. After passing point B_{16}, the wall shear stress suddenly decreases and approaches the asymptotic value τ_D.

The present LDV system can measure the velocity profile at the sections P_1 and M_1 immediately downstream of the flow divider by 0·5 mm where wall shear stress reaches a value several times larger than that upstream in the parent tube. Along the distal wall (E_i, □), wall shear stress steeply decreases from the value $\tau_w = 8$ at section M_1 near the flow divider and approaches the asymptotic value τ_D. Also, along the inner wall (F_i, ◇), wall shear stress steeply decreases from $\tau_W = 6$ at section P_2 near the flow divider and asymptotically approaches τ_P.

When comparing the results obtained by the two methods, the general trends of wall shear stress measured by the electrochemical method agree well with those calculated from the velocity. Particularly, at the transition point B_{16} from the straight upstream parent tube to the round upstream corner as shown in Figure 7(a), wall shear stress measured by the electrochemical method coincides with that calculated from the velocity. On the other hand, there is some discrepancy along the proximal wall from B_{18} to B_{23}. Also, the difference between LDV and electrochemical measured shear stress is large along the distal and the inner walls around the flow divider. These discrepancies are likely related to errors in the electrochemical method.

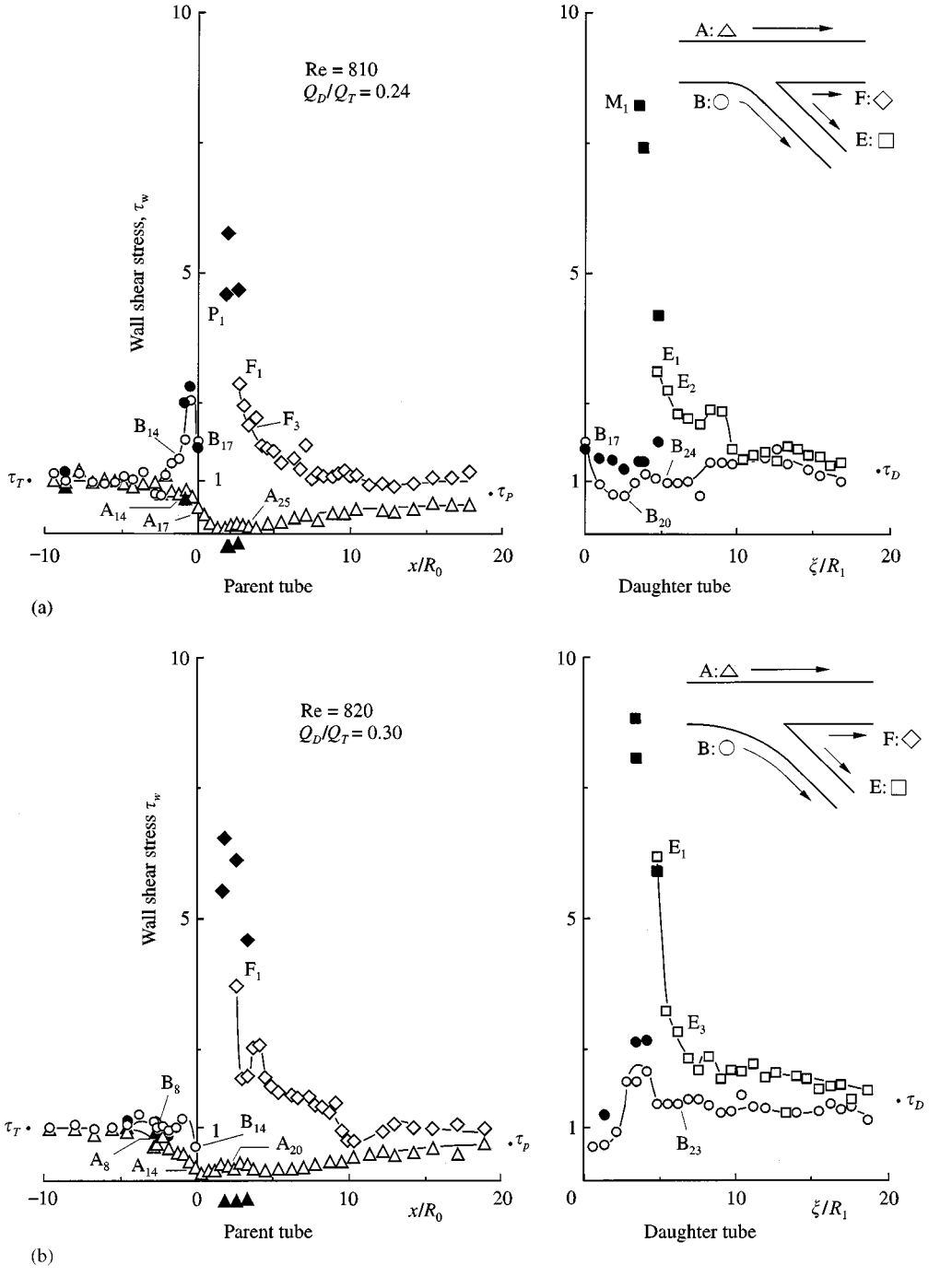

Figure 7. Comparison of wall shear stress estimated from velocity profile with that measured by electrochemical method in steady flow. Open and closed symbols denote the wall shear stress measured by electrochemical method and that estimated from velocity profile, respectively. (a) Distribution of wall shear stress for $R_D = D_0$; (b) distribution of wall shear stress for $R_D = 3{\cdot}5D_0$.

An error estimation is performed in the Poiseuille flow of the upstream parent tube. In Figure 7(a), flow between positions A_1, B_1 and A_{12}, B_{12} is approximately Poiseuille flow. Consequently, the wall shear stress at these positions should be $\tau_w = 1{\cdot}0$. However, there is large scatter in the measured value of wall shear stress at several positions. From the comparison of the wall shear stress at these positions with that of the Poiseuille flow, the characteristic error attributed to the electrochemical probe shear measurement would be approximately 15%. Also, the wall shear stress measured by the electrochemical method is the spatial averaged value across the probe diameter of 0·5 mm. If the wall shear stress at M_1, M_2, and M_3 measured by LDV is correct, the error due to the spatial average across the probe diameter of 0·5mm can be estimated to be approximately 5% from the gradient of wall shear stress in Figure 7(a). However, the discrepancy along positions B_{18}–B_{23} is much greater than the estimated error of 15%. Second possible explanation comes to mind. In general, flow separation is apt to occur along the proximal wall in a two-dimensional branch. Even in a three-dimensional branch, the region from positions B_{18}–B_{23} is a very sensitive flow field. Furthermore, it is not possible to embed the electrode used in the electrochemical method exactly at the common median plane. As indicated in the previous paper (Yamaguchi & Kohtoh 1994), the centre of electrode deviates by 0·75 mm (6°) from this plane. Although it is difficult to quantify the effects of those two factors, they could conceivably explain the discrepancy along positions B_{18}–B_{23}

The radius of curvature at the upstream corner affects variation of wall shear stress around the transition point from the straight upstream parent tube to the round upstream corner. In the case of $R_D = D_0$ as shown in Figure 7(a), the wall shear stress reaches the maximum value $\tau_w = 2{\cdot}5$ around the transition point B_{16}. On the other hand, in the case of $R_D = 3{\cdot}5D_0$ as shown in Figure 7(b), the maximum value of wall shear stress does not appear around the transition point B_8. Therefore, the wall shear stress around the transition point has a clear maximum value as the radius of curvature R_D becomes smaller.

4. GENERAL FLOW STRUCTURE THROUGH ASYMMETRICAL BRANCH, ITS PHYSIOLOGICAL MEANING AND CONCLUSION

The present branch model simulates arterial flow from the abdominal aorta to the inferior mesenteric artery. According to the study by Yamaguchi *et al.* (1986), the diameter of the abdominal aorta and the inferior mesenteric artery in humans are $D_0 = 6{\cdot}3$ mm and $D_1 = 2{\cdot}6$ mm, respectively. The diameter ratio of $D_1/D_0 = 0{\cdot}58$ in the present branch model is a little different from that in the physiological condition of $D_1/D_0 = 0{\cdot}41$. However, from the flow situation of the present model, fundamental flow characteristics such as the velocity profile and the distribution of wall shear stress through the asymmetrical branch could be estimated. According to Yamamoto *et al.* (1992), flow through the abdominal aorta can be approximated as flow with the Womersley number less than 6. In pulsatile flow significant inertial effects and secondary flows would exist. These steady-state results provide a useful first step toward understanding the phenomena in pulsatile flow.

From flow visualization and velocity profile measurement, the flow structure sketched in Figure 8 is obtained. The flow segment at the upstream section flowing into both downstream tubes is indicated in the top of Figure 8(a) and the path line around the branch point is also indicated in the bottom of Figure 8(a). Fluid entering from the upstream parent tube is divided into two parts, i.e., the dense and light hatched regions which flow into the daughter tube and the downstream parent tube, respectively. Fluid passing through the dense hatched eccentric region along the tube wall having little momentum basically impinges on the round upstream corner and flows into the daughter tube. The fluid occupying the core region bifurcates into two parts after passing the flow divider. Fluid

from the densely hatched core flows into the daughter tube as a pair of the secondary helical flows which is symmetrical with respect to the common median plane. The lightly hatched core fluid enters into the downstream parent tube.

In order to explain the path line of a fluid particle, the path lines in the bottom of Figure 8(a) are numbered. Path line "1" entering the daughter tube along the common

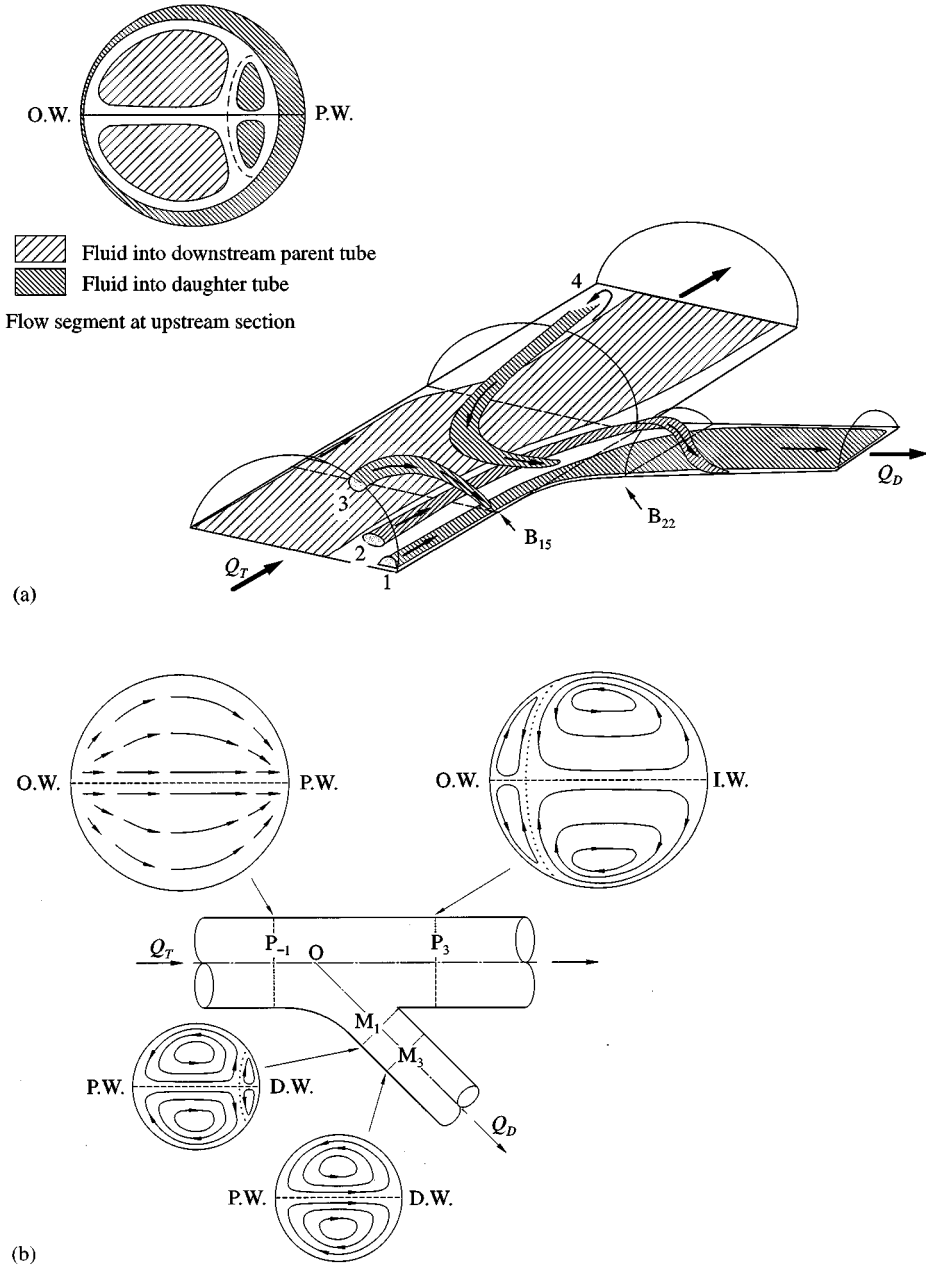

Figure 8. Sketch of flow field in asymmetrical branch model (Re = 800, $Q_D/Q_T = 0{\cdot}24$, $R_D = D_0$): (a) main flow field; (b) secondary flow at typical section.

median plane moves towards the distal wall at the common median plane. However, this path line "1" does not travel in a helical motion in the daughter tube, and simply spreads at the common median plane in the daughter tube. The path lines travelling in a helical motion due to secondary flow are "2", "3", and "4". After passing the flow divider, path line "2" travels in a helical motion in the daughter tube. Path line "3", originating near the peripheral tube wall close to the common median plane, impinges near position B_{15}. Path line "4", coming from the separation zone in the parent tube, goes upstream along the peripheral tube wall and travels in a helical motion due to secondary flow in the daughter tube.

The secondary flow pattern is sketched in Figure 8(b). Another small region of secondary flow appears at section M_1 near the flow divider along the distal wall in the daughter tube. Also, there is a small region of secondary flow within the separation region along the outer wall downstream of the parent tube.

The variation of wall shear stress along the proximal wall is closely associated with these secondary flows. A maximum exists around B_{16} along the proximal wall as shown in Figure 7(a). This maximum value of wall shear stress at B_{16} is induced by the secondary flow, the dense hatched eccentric fluid along the peripheral tube wall with small momentum, which impinges to the round upstream corner from the parent tube. Therefore, it appears that the variation of wall shear stress around the upstream corner is closely related to the secondary flow from the parent tube.

Atherosclerotic disease has been observed at the entrance of the daughter tube along the proximal wall of the abdominal aorta according to Cornhill *et al.* (1980), Kjaernes *et al.* (1981), Friedman *et al.* (1981), Yamaguchi *et al.* (1986) and Yoshida *et al.* (1987). It has generally been considered that the magnitude of the wall shear stress is low along the proximal wall in a two-dimensional branch flow and that the mass transfer rate dependent on the shear rate is consequently lower at this region. However, in a three-dimensional branch flow, the wall shear stress clearly increases above the upstream value approaching the entrance of the daughter tube, and varies along the proximal wall with a peak maximum value around the transition point B_{16}. This behaviour would suggest that these variations in wall shear stress might have implications for the development of atherosclerotic disease in terms of their influence on phenomena such as endothelial cell orientation, the mass transport across the endothelial cell, and the cell function.

ACKNOWLEDGEMENTS

This research has been supported by the Japanese Ministry of Education, Science, Sports and Culture, Grant-in-Aid for Scientific Research (B) #09450083. The author is grateful to thank to Mr Kenji Kohtoh for his helpful assistance.

References

Cornhill, J. F., Levesque, M. J. & Nerem, R. M. 1980 Quantitative study of the localization of sudanophilic coeliac lesions in the white carneau pigeon. *Atherosclerosis* **35,** 103–110.

El Masry, O. A. & Feuerstein, I. A. 1982 Electrochemical surface shear rate evaluation in models of the renal artery. *ASME Journal of Biomechanical Engineering* **104,** 290–295.

Friedman, M. H., Hutchins, G. M., Bargeron, B. C., Deters, O. J. & Mark, F. F. 1981 Correlation between intimal thickness and fluid shear in human arteries. *Atherosclerosis* **39,** 425–436.

Kjaernes, M., Svindland, A., Walloe, L. & Wille, S. O. 1981 Localization of early atherosclerotic lesions in an arterial bifurcation in humans. *Acta Pathologia et Microbiologica Scandinavia*, Section A **89,** 35–40.

KU, D. N., GIDDENS, D. P., CHRISTOPHER, K. Z. & GLAGOV, S. 1985 Pulsatile flow and atherosclerosis in the human carotid bifurcation. *Arteriosclerosis* **5,** 293–302.

LUTZ, R. J., CANNON, J. N., BISCHOFF, K. B., DEDRICK, R. L., STILES, R. K. & FRY, D. L. 1977 Wall shear stress distribution in a model canine artery during steady flow. *Circulation Research* **41,** 391–399.

MCDONALD, D. A. 1974 *Blood Flow in Arteries*, pp. 92–95, London: Edward Arnold.

MIZUSHINA, T. 1971 The electrochemical method in transport phenomena. In *Advances in Heat Transfer*, Vol. 7, pp. 87–161, London: Academic Press.

RODKIEWICZ C. M., & ROUSSEL, C. L. 1973 Fluid mechanics in a large bifurcation. *ASME Journal of Fluids Engineering* **95,** 108–112.

STEHBENS, W. E. 1959 Turbulence of blood flow. *Quarterly Journal of Experimental Physiology* **44,** 110–117.

YAMAGUCHI, R. 1989 Distribution of mass transfer rate and wall shear stress behind simple rectangular stenosis in pulsating flow. *ASME Journal of Biomechanical Engineering* **111,** 47–54.

YAMAGUCHI, R. & KOHTOH, K. 1994 Sinusoidal variation of wall shear stress in daughter tube through 45 deg branch model in laminar flow. *ASME Journal of Biomechanical Engineering* **116,** 119–126.

YAMAGUCHI, T., HANAI, S., OYAMA, T., MITSUMATA, M. & YOSHIDA, Y. 1986 Effect of blood flow on the localization of fibrocellular intimal thickening and atherosclerosis at the young human abdominal aorta-inferior mesenteric artery branching. *Recent Advances in Cardiovascular Disease* **7-1**, 97–108 (in Japanese).

YAMAMOTO, T., TANAKA, H., JONES, C. H. J., LEVER, M. J., PARKER, K. H., KIMURA, A., HIRAMATSU, O., OGASAWARA, Y., TSUJIOKA, K., CARO, C. C. G. & KAJIYA, F. 1992 Blood velocity profiles in the origin of the canine renal artery and their relevance in the localization and development of atherosclerosis. *Arteriosclerosis and Thrombosis* **12,** 626–632.

YOSHIDA, Y., OYAMA, T., WANG, S., YAMANE, T., MITSUMATA, M., YAMAGUCHI, T. & ONEDA, G. 1987 Underlying morphological changes in the arterial wall at bifurcations for atherogenesis. In *Role of Blood Flow in Atherogenesis*, pp. 33–40. Berlin: Springer-Verlag.